

Self-Assembly



# Room-Temperature Ice Growth on Graphite Seeded by Nano-Graphene Oxide\*\*

Yi Zheng, Chenliang Su, Jiong Lu, and Kian Ping Loh\*

Water wetting on a hydrophobic surface at ambient conditions is disallowed by the non-polar nature of the surface and high vapor pressure of water.<sup>[1–3]</sup> However, the presence of sub-millimeter sized hydrophilic patches allows the waxy wings of desert beetles to become wettable by morning mist.<sup>[4,5]</sup> Herein, we show that a sprinkle of graphene oxide nanoflakes (nanoGOs) is effective in condensing water nanodroplets and seeding ice epitaxy on graphite at ambient conditions. By controlling the relative humidity and nanoGO density, we are able to study the formation of a complete ice wetting layer on a time scale of 20 h. This presents an unprecedented opportunity to visualize ice nucleation and growth in real time using non-contact atomic force microscopy. The stages of crystallization, as proposed by Ostwald in 1897,<sup>[6]</sup> are fully unfolded at a microscopic level for the first time. We obtain real-time imaging of the sequential phase transition from amorphous ice to a transient cubic ice  $I_c$  stage, and finally to the stable hexagonal ice  $I_h$ . Most interestingly, we discover that ice nucleation and growth can be influenced by modifying the functional groups of nanoGO and by intermolecular hydrogen-bonding between nanoGOs. This affords a strategy to control heterogeneous ice nucleation and snow crystal formation.<sup>[7,8]</sup>

The interaction of water with solid surfaces is one of the most pervasive natural phenomena which underpins, for example, rain precipitation, snow formation, rock erosion. The wetting of surfaces by ambient water is also of crucial importance in many processes, such as heterogeneous catalysis, photocatalysis, microelectronics, and drug development.<sup>[1,3]</sup> In bulk ice which is formed below 0°C, water molecules pack in a hexagonal ice  $I_h$  structure with four hydrogen bonds arranged in tetrahedral geometry.<sup>[8]</sup> Above 0°C, vibrational lattice instability leads to the liquid phase.<sup>[9,10]</sup> A new idea emerged recently, that the ice-to-liquid phase transition crossing the freezing point may not apply in the two dimensional (2D) limit. Recent research revealed that at a hydrophilic interface,<sup>[11]</sup> or by nanoconfinement,<sup>[12,13]</sup> ice  $I_h$  wetting layers can persist even at

ambient conditions. To date, insights into the hydration structure and wetting dynamics of ambient water on solids is derived mainly from studies on single-crystal metal surfaces carried out at cryogenic temperatures in vacuum conditions.<sup>[1,3,14]</sup> Molecular level studies of water/ice nucleation and growth on solid surfaces at ambient conditions remain a formidable challenge owing to the highly mobile nature of water molecules and its high vapor pressure.<sup>[2]</sup>

In our ice growth experiments, we use nanoGOs as ice nucleation seeds. These nanoGOs were heated in base and had a higher degree of restored  $sp^2$  conjugation than the as-synthesized nanoGOs as well as carboxylate ( $COO^-$ ) groups on their periphery, as shown by vibrational spectroscopy (Figure S1 in the Supporting Information). After spin coating nanoGOs on a freshly peeled highly ordered pyrolytic graphite (HOPG), the samples were dried at 80°C for 15 min before amplitude-modulated non-contact atomic force microscopy (NCAFM) imaging.<sup>[15]</sup> The typical NCAFM amplitude setpoint for direct imaging of ice epitaxial domains is 2–3 nm. Using higher setpoints results in a perturbation of the wetting layer or even penetration of the water films (see Figure S2 for setpoints of 6 nm and > 10 nm). Penetration allows us to directly image the underlying substrate and determine the physical dimensions of nanoGOs, which have heights varying from 0.5 nm to several nm (Figure S2 and S3).

Figure 1a illustrates the dynamic processes involved in room-temperature ice formation on graphite seeded by superhydrophilic nanoGOs. We modify the graphite substrate with 1–10% surface coverage of nanoGOs. The advantages of using the graphite surface as a template include its atomic flatness which does not disrupt the fragile hydrogen bonding in ice structures, and its ability to conduct the latent heat produced by ice condensation rapidly. The triangular sublattice of graphite (2.46 Å) matches the natural ice structure very well. All these factors favor the epitaxial growth of a commensurate ( $\sqrt{3} \times \sqrt{3}$ )R30° ice  $I_h$  overlayer.<sup>[16,17]</sup> However, under ambient conditions, the formation of 2D ice overlayers on graphite is suppressed by strong sublimation arising from the high vapor pressure of water (19.5 Torr),<sup>[2]</sup> and no large-area water condensation is observed on bare graphite (Figure 1b). This difficulty can be circumvented by the fast surface diffusion of water molecules<sup>[18]</sup> from scattered nanodroplet reservoirs, which are readily clustered on nanoGOs at a relative humidity (RH) as low as 15%. As illustrated in Figure 1a, liquid droplets can be efficiently captured by the strongly hydrophilic carboxylate groups of the nanoGOs. Surface tension leads to the formation of near-spherical nanodroplets covering the underlying nanoGOs, with a typical liquid thickness of approximately 0.5 nm (Figure S2 and S3).

[\*] Dr. Y. Zheng, Dr. C. Su, Dr. J. Lu, Prof. K. P. Loh  
Department of Chemistry and Graphene Research Centre  
National University of Singapore  
3 Science Drive 3, Singapore (Singapore)  
E-mail: chmllohkp@nus.edu.sg

[\*\*] K.P.L. acknowledges funding support from Singapore Millenium Foundation Research Horizon Award R-143-000-417-133 as well as Economic Development Board (SPORE, COY-15-EWI-RCFSA/N197-1). Discussion with Prof. A. H. Castro Neto is gratefully acknowledged.



Supporting information for this article is available on the WWW under <http://dx.doi.org/10.1002/anie.201302608>.

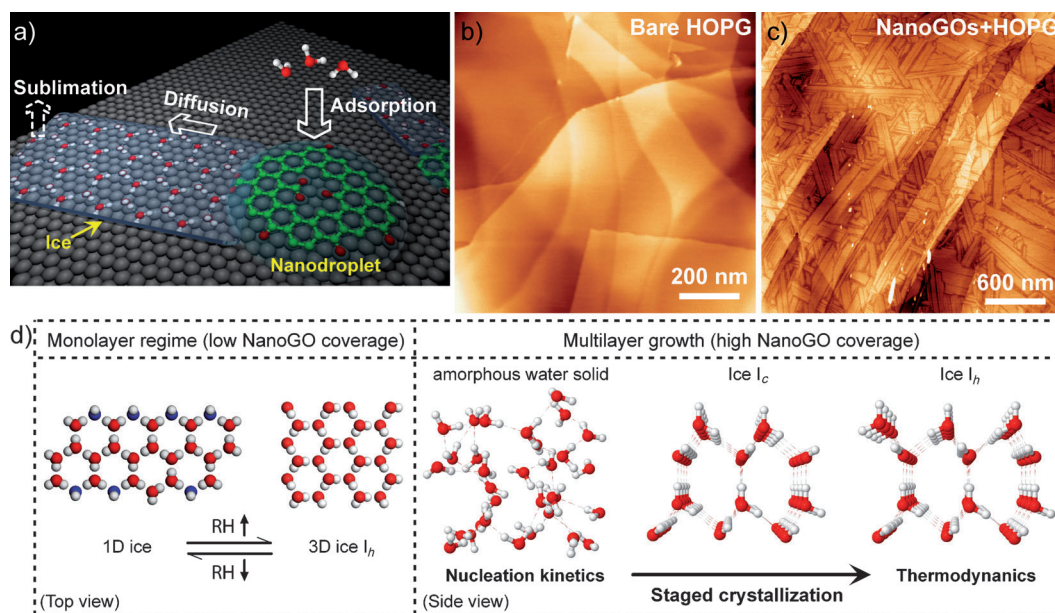


**Figure 1.** Ice formation on graphite surface at ambient conditions seeded by superhydrophilic nanoGOs. a) Schematic representation of ice formation on graphite, nucleated by the carboxylate functional groups of nanoGOs. The coverage of ice domains on graphite is determined by dynamic balance between water adsorption on nanoGOs and sublimation on graphite. H white O red. b),c) NCAFM topography images: b) Without nanoGOs, water does not condense on graphite. Color scale: dark to light 0–2 nm. c) High coverage of ice wetting layers formed on graphite in few minutes due to exposure to high humidity levels. Color scale: dark to light 0–3 nm. d) Summary of ice formation on graphite as a function of relative humidity (RH) and nanoGO density, see text for details. Dashed lines are hydrogen bonds.

The negatively charged carboxylate groups provide the first anchor site for ice nucleation (Figure 1a). From these, the growth of ice crystals is driven by the outward diffusion of water from the nanoGOs. The final coverage of ice domains is a dynamical balance between water adsorption on nanoGOs and sublimation on graphite surface (Figure 1a), which can be controlled by tuning the RH and nanoflake density. At high humidity levels (RH > 70%), the graphite surface is quickly covered by ice crystalline domains in a few minutes. Figure 1c shows a characteristic NCAFM image of large-area ice thin film formed on HOPG. It has to be emphasized that the surface of the ice overlayers is imaged directly, in contrast to the recent report of nano-confined ice sandwiched between graphene and mica.<sup>[13]</sup> The direct imaging provides molecular-level lateral resolution and allows the ice nucleation and growth process to be studied. For instance, we are able to observe reversible phase transition between an unconventional 1D ice structure and ice  $I_h$  (left panel of Figure 1d). At a high nanoGO coverage, we can observe a non-reversible staged crystallization in multilayer ice growth (right panel of Figure 1d), which is fully revealed for the first time since proposed by Ostwald in 1897.<sup>[6]</sup>

Figure 2a shows a typical NCAFM image of the first ice wetting layer on HOPG, seeded by low density nanoGOs (ca. 0.9% coverage) at a low RH of 16%. These ice domains are around 0.3 nm in height and consist of periodical 1D chains (the inset of Figure 2a). The measured step height is significantly smaller than the optimized distance between an ice  $I_h$  monolayer and graphite (0.38 nm),<sup>[16]</sup> but agrees with an ice overlayer with water molecules lying flat on the surface.

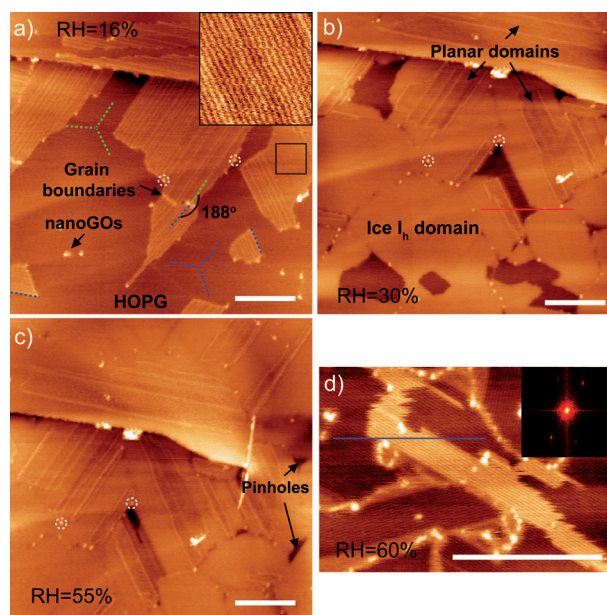


**Figure 2.** NCAFM topography images of the first room-temperature ice wetting layer. a) Submonolayer ice domains at 16% RH. Inset: expansion of the periodical 1D ice. Green and blue highlight two crystallographic directions miss-oriented by 8°. b) Faceted ice  $I_h$  domain formation with larger adsorption flux at 30% RH. c) At 55% RH, HOPG is nearly fully covered by ice. d) Formation of a second coplanar submonolayer, hydrogen bonded to the underlying ice domain (for line profile (blue) see Figure S6). Inset: fast Fourier transform of (d), showing two 1D ice orientations. Scale bars are 200 nm. Dashed white circles are the coordination reference point. Color scale: dark to light a)–c) 0–1.4 nm; d) 0–1 nm.

The formation of a flat-lying phase at low RH can be rationalized by the maximization of hydrogen-bonding between neighboring water molecules to stabilize ice domains against increasing sublimation. Unlike the tetrahedral hydrogen-bonding in ice  $I_h$  which can extend infinitely (3D icing; see Figure S4), such coplanar adsorption breaks translational symmetry and can only form clusters or narrow stripes, determined by the “2D ice rule”.<sup>[19]</sup> As illustrated in Figure 1d, beyond the first flat-lying hexamer, adding each hex-

agon will introduce one defect site, on which water molecules will accept two H-bonds but donate none for intermolecular H-bonding. Consequently, water molecules at the defect site (oxygen in blue in Figure 1 d) have their plane vertical to the surface, which disfavors further intermolecular H-bonding.<sup>[19]</sup>

Energy minimization gives rise to the periodical 1D chain structure with defect molecules on the periphery. The orientations of the 1D chains are characterized by a pronounced threefold symmetry (dashed lines in Figure 2 a). The symmetry originates in the  $\pi$ - $\pi$  coupling between nanoGO backbone and graphite. NanoGOs are effective in nucleating ice, but nucleation rarely happens for GO flakes larger than 100 nm (Figure S5). By increasing RH to 30%, isolated ice domains surrounding nanoGOs expanded and formed a continuous wetting layer (Figure 2b). Unlike the case in Figure 2a, the wetting layer at 30% RH has predominantly smooth surfaces although some local areas retain the periodical 1D structure. With a further increase in RH to 55%, graphite is fully covered by the wetting layer except for some non-coalescent pinholes (Figure 2c). The step height of the smooth domains is consistent with one ice  $I_h$  monolayer on HOPG ( $0.38 \pm 0.02$  nm; Figure S6). The phase image also confirms that this new phase is the first ice  $I_h$  monolayer, as manifested by its distinct phase contrast from graphite (Figure S7). The observation implies that at higher humidity, the ice  $I_h$  structure becomes kinetically favored because of the higher packing density of water molecules. Above 55% RH, a second coplanar adlayer can be observed occasionally (Figure 2d). This second layer is hydrogen bonded to the underlying ice wetting layer as indicated by the measured step height of 0.38 nm (Figure S6). However, in general, we did not observe the full coalescence of 1D chains into ice  $I_h$  monolayer.

Although the phase transition between 1D ice and ice  $I_h$  monolayer is driven kinetically by packing density and is reversible, the natural ice structure becomes energetically favorable once multilayer ice is formed. This change is attributed to the formation of interlayer hydrogen bonding, which compensates the energy cost of vertical buckling of approximately 0.1 nm between neighboring water molecules.<sup>[3]</sup> Multilayer ice can be grown on graphite by increasing the nanoGO coverage to enhance the water adsorption flux. At an intermediate RH of 40% and at nanoGO density of 4%, it takes 24 h to form a continuous ice thin film, which allows the real-time wetting dynamics to be recorded by NCAFM (20 mins per image). As shown in Figure 3 a–e, the growth of ice multilayers on graphite under these conditions is highly anisotropic. The fast growth directions of each ice crystal follow the threefold symmetry as determined by the underlying graphite (dashed lines in Figure 3 a).

By tracking the step heights of individual ice crystals as a function of time, we found that in the beginning, the majority of freshly nucleated crystals are amorphous solid water (ASW) instead of ice  $I_h$ . This is manifested by a ( $0.68 \pm 0.02$ ) nm step height which disagrees with multiples of ice  $I_h$  monolayer (Figure 3 f and raw data in Figure S8). This polymorph contains voids and dangling hydrogen bonds (Figure 1 d), and has minimum activation energy for nucleation owing to its structural similarity to the liquid phase.<sup>[14]</sup>

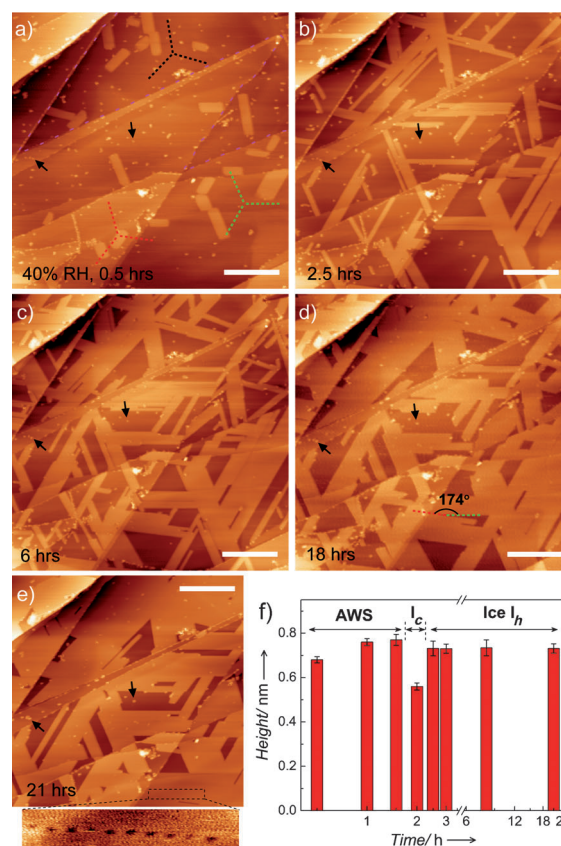


**Figure 3.** Real-time ice growth on HOPG at 40% RH, seeded by 4% of nanoGOs. a) NCAFM topography image right after the baking, showing threefold ice crystal growth in relation to graphite. Three crystallographic directions (dotted lines) are determined using the orientation of ice crystals (black arrows indicate two nanoGOs which do not initiate ice growth after 21 h) after b) 2.5 h, c) 6 h, d) 18 h, e) 21 h. Inset: expansion of highlighted region showing the coalescence of two small mismatched ice domains forming a 1D array of triangular pinholes. Scale bars are 500 nm. Color scale: from dark to light 0–4.5 nm. f) Step-height analysis of an ice domain as a function of time, showing polymorphism evolution from amorphous solid water (AWS) to ice  $I_c$ , and finally to ice  $I_h$ .

The ASW phase slowly develops after 1.5 h into another metastable phase with a step height of ( $0.56 \pm 0.02$ ) nm (Figure 3 f and Figure S8). Noticeably, the thickness of 0.56 nm corresponds to two hexagonal monolayers of ice  $I_c$  phase.<sup>[20,21]</sup> Consistent with previous water freezing experiments,<sup>[20]</sup> such an ice  $I_c$  phase is transient and quickly evolves into ice  $I_h$  within half an hour (Figure 3 f and Figure S8). The staged crystallization from the less-stable polymorphs (ASW followed by ice  $I_c$ ) to the most stable ice  $I_h$  was proposed by Ostwald as an empirical rule in 1897,<sup>[6]</sup> and is related to the nucleation kinetics of solid phase from liquid phase.<sup>[22,23]</sup>

The presence of carboxylate groups on the edges of base-treated nanoGOs plays a key role in ice nucleation. This can be rationalized by the enhanced electrostatic interactions between the charged H-acceptor  $\text{COO}^-$  and water molecules, a phenomenon known as “charge-assisted hydrogen bonding”.<sup>[24]</sup> In  $\text{COO}^-$ , the negative charge is delocalized between two oxygen atoms in a resonance structure, creating two

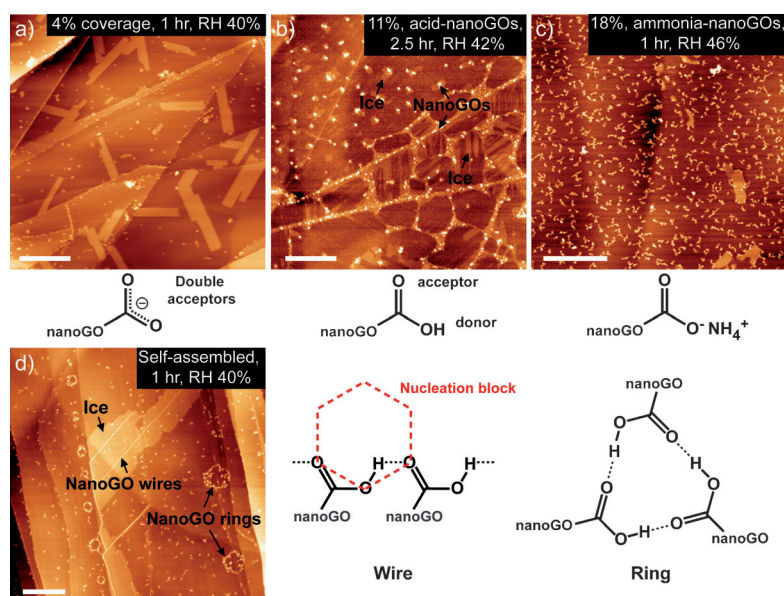


**Figure 4.** Tuning ice nucleation and growth by modifying the functional groups and by self-assembly of nanoGOs. a) Typical anisotropic ice growth nucleated by negatively charged carboxylate groups. b) After acid neutralization, ice nucleation is suppressed. c) Charge neutralization by treatment of nanoGOs with ammonia solution. The result is consistent with the acid treatment. d) Left: Quasi-isotropic ice growth nucleated by self-assembled 1D nanoGO wires. Right: possible hydrogen-bonding configuration in 1D wires and carboxylic rings. Scale bars are 500 nm. All images are topography. Color scale: from dark to light a) 0–4.5 nm; b) and c) 0–1.5 nm; d) 3 nm.

strong hydrogen-bond acceptors (Figure 4a). The resulting ice nucleation starts immediately after the baking process, and the ice growth is highly anisotropic (Figure 4a). In contrast, acid treated nanoGOs are much weaker in initiating ice growth, even when the coverage is significantly increased (Figure 4b). Interestingly, treating with ammonia results in the formation of self-assembled nanoGO structures, possibly by charge-assisted hydrogen bonding between  $\text{NH}_4^+$  and the carboxylate groups in nanoGOs. This effectively reduces the density of free carboxylate groups for hydrogen bonding with water, thus ice growth is suppressed (Figure 4c). By allowing nanoGOs to self-assemble on graphite by hydrogen bonding, the anisotropic ice nucleation can be transformed into quasi-isotropic. As shown in Figure 4d, nanoGOs can form 1D wires and seed ice growth around the wire backbones. In contrast, the self-assembled ring structures do not favor ice nucleation. This difference can be explained in that 1D hydrogen bonding of carboxylic groups provides a building block with structural similarity to ice hexamer, which effectively promotes ice nucleation (Figure 4d). However, the intermolecular association of ring structures in general does not provide such active sites for ice nucleation. For example, the strong linear hydrogen bonding in a triple-carboxylic ring makes the  $\text{C}=\text{O}$  acceptor disfavor forming a second hydrogen-bond, which requires a change in the acceptor directionality from linear to about  $120^\circ$  (see a six-carboxylic ring in Figure S9).

It is remarkable that very low surface coverage of nanoGOs can transform the water wetting dynamics on

a macroscopically large hydrophobic surface and effectively promote ice formation even at ambient conditions. This result has implications for engineering wetting on a wide range of surfaces for anti-fogging or anti-fouling applications.<sup>[25]</sup> NanoGOs combine the advantages of transparency and water-solubility and can be readily sprayed, rolled, printed, screen casted, and are thus amenable to large area surface-treatment technologies. At a fundamental level, we show that the hybrid nanoGO-graphite template can be used as a model system to study crystal nucleation and growth in real time. By engineering the functional groups on nanoGOs and introducing different chemical modifications, the long-debated heterogeneous ice nucleation and snow-crystal formation could be better understood at a molecular level. Using frequency modulated NCFM and Kelvin probe microscopy,<sup>[26]</sup> it would be possible to study the molecular structure of these room temperature ice thin films. Finally, the implication for graphene<sup>[27,28]</sup> electronics is that the formation of ice-like clusters may occur near defects and oxygenated adsorbates in humid conditions. These phenomena may influence the electronic properties.

Received: March 28, 2013

Revised: May 19, 2013

Published online: July 3, 2013

**Keywords:** atomic force microscopy · hydrophobic surfaces · ice · nano graphene oxide · phase transitions

- [1] P. A. Thiel, T. E. Madey, *Surf. Sci. Rep.* **1987**, *7*, 211–385.
- [2] A. Verdager, G. M. Sacha, H. Bluhm, M. Salmeron, *Chem. Rev.* **2006**, *106*, 1478–1510.
- [3] P. J. Feibelman, *Phys. Today* **2010**, *63*, 34–41.
- [4] A. R. Parker, C. R. Lawrence, *Nature* **2001**, *414*, 33–34.
- [5] L. Zhai, M. C. Berg, F. C. Cebeci, Y. Kim, J. M. Milwid, M. F. Rubner, R. E. Cohen, *Nano Lett.* **2006**, *6*, 1213–1217.
- [6] W. F. Ostwald, *Z. Phys. Chem.* **1897**, *22*, 289–330.
- [7] K. G. Libbrecht, *Rep. Prog. Phys.* **2005**, *68*, 855–895.
- [8] *The Chemical Physics of Ice* (Ed.: N. H. Fletcher), Cambridge Univ. Press, London, **1970**.
- [9] P. Wernet, D. Nordlund, U. Bergmann, M. Cavalleri, M. Odelius, H. Ogasawara, L. A. Naslund, T. K. Hirsch, L. Ojamae, P. Glatzel, L. G. M. Pettersson, A. Nilsson, *Science* **2004**, *304*, 995–999.
- [10] J. D. Smith, C. D. Cappa, K. R. Wilson, B. M. Messer, R. C. Cohen, R. J. Saykally, *Science* **2004**, *306*, 851–853.
- [11] J. Hu, X. D. Xiao, D. F. Ogletree, M. Salmeron, *Science* **1995**, *268*, 267–269.
- [12] K. B. Jinesh, J. W. M. Frenken, *Phys. Rev. Lett.* **2008**, *101*, 036101–036104.
- [13] K. Xu, P. Gao, J. R. Heath, *Science* **2010**, *329*, 1188–1191.
- [14] A. Hodgson, S. Haq, *Surf. Sci. Rep.* **2009**, *64*, 381–451.
- [15] Y. Martin, C. C. Williams, H. K. Wickramasinghe, *J. Appl. Phys.* **1987**, *61*, 4723.
- [16] T. O. Wehling, A. I. Lichtenstein, M. I. Katsnelson, *Appl. Phys. Lett.* **2008**, *93*, 202110.

- [17] O. Leenaerts, B. Partoens, F. M. Peeters, *Phys. Rev. B* **2009**, *79*, 235440.
- [18] F. Sciortino, A. Geiger, H. E. Stanley, *Nature* **1991**, *354*, 218–221.
- [19] M. Tatarkhanov, D. F. Ogletree, F. Rose, T. Mitsui, E. Fomin, S. Maier, M. Rose, J. I. Cerda, M. Salmeron, *J. Am. Chem. Soc.* **2009**, *131*, 18425–18434.
- [20] B. J. Murray, A. K. Bertram, *Phys. Chem. Chem. Phys.* **2006**, *8*, 186–192.
- [21] T. L. Malkin, B. J. Murray, A. V. Brukhno, J. Anwar, C. G. Salzmänn, *Proc. Natl. Acad. Sci. USA* **2012**, *109*, 1041–1045.
- [22] *Kinetic der Phasenbildung* (Ed.: M. Volmer), Steinkopf, Leipzig, **1939**.
- [23] *Polymorphism in Molecular Crystals* (Ed.: J. Bernstein), Clarendon Press, Oxford, **2002**.
- [24] M. Steiner, *Angew. Chem.* **2002**, *114*, 50–80; *Angew. Chem. Int. Ed.* **2002**, *41*, 48–76.
- [25] R. Wang, K. Hashimoto, A. Fujishima, M. Chikuni, E. Kojima, A. Kitamura, M. Shimohigoshi, T. Watanabe, *Nature* **1997**, *388*, 431–432.
- [26] a) T. Fukuma, M. J. Higgins, S. P. Jarvis, *Phys. Rev. Lett.* **2007**, *98*, 106101; b) C. Barth, A. S. Foster, C. R. Henry, A. L. Shluger, *Adv. Mater.* **2011**, *23*, 477–501.
- [27] A. K. Geim, K. S. Novoselov, *Nat. Mater.* **2007**, *6*, 183–191.
- [28] A. H. Castro Neto, F. Guinea, N. M. Peres, K. S. Novoselov, A. K. Geim, *Rev. Mod. Phys.* **2009**, *81*, 109–162.
-